

1 Possible Titles

Elastodynamic and hydraulic properties of fractured and sheared rock: An experimental investigation

Imaging elastodynamic and hydraulic properties of in-situ fractured rock: An experimental investigation considering effects of dynamic stressing and shearing

2 Abstract

We describe laboratory work to elucidate the relationship between nonlinear elasticity and permeability of fractured media subjected to local stress perturbations in relation to fracture roughness and aperture distribution. This study is part of an effort to image fluid pathways and fracture properties using locally induced seismicity, associated with fluid injection. Experiments were conducted in which intact L-shaped Westerly Granite samples were fractured in-situ tri-axial conditions while forcing deionized water through the subsequent fracture interfaces. After in-situ fracture, we imposed oscillations of the applied Normal stress and pore pressure with amplitudes ranging from 0.2 to 1 MPa and frequencies from 0.1 to 10 Hz. During these dynamic perturbations an array of ultrasonic transducers (PZTs) continuously generated and transmitted p-wave pulses to monitor the elastic response of the granite samples. We interpret the relative change in p-wave velocities to be an analog for the elastic non-linearity and relate it to the permeability of the fractured media. The roughness of the fracture interfaces is altered during experiments by shearing the L-shaped samples and then allowing the interface to age before applying dynamic stressing. We observe changes in the permeability and stiffness of the fracture during the dynamic perturbations and also with the shearing history, changing roughness, of the Westerly Granite samples.

3 Introduction

Dynamic stresses associated with energy production and waste water sequestration (injection, pumping, and transport of supercritical H_2O-CO_2 fluids) are particularly concerning as they are known to induce seismicity [Healy et al., 1968; Raleigh et al., 1976; Simpson et al., 1988; Sminchak and Gupta, 2003; McNamara et al., 2015; McGarr et al., 2015; Walsh and Zoback, 2015].

Though dynamic stressing could be beneficial for enhanced permeability, it presents a significant risk associated with fault reactivation, reservoir seal damage, and accelerated deformation. Therefore, it is important to understand how fluid injection influences the hydromechanical properties of rocks and fractures. We have performed careful laboratory experiments to investigate the connection between fluid flow and elastic nonlinearity (i.e. stress is not proportional to strain) of fractured media.

Dynamic stressing of the local subsurface associated with seismicity, drilling, hydraulic injection cause transient changes in permeability. These perturbations cause significant changes in the local stress field and consequently the poromechanical properties of the local subsurface. Empirical evidence from the field and laboratory show that earthquakes and subsequent seismic waves cause transient changes in rock stiffness in the proximity of faults. Specifically, measurements of a sudden decrease in seismic wave velocity from coseismic softening and a post-seismic relaxation of the rock stiffness, a logarithmic recovery in time. Scaling down to laboratory studies, it has been shown that by using dynamic acousto-elastic testing, ultrasonic wave velocity (analog for field-scale seismometers) recorded decreased during dynamic stressing and then recovered after dynamic stressing ended with a logarithmic form. Dynamic perturbations with strain on the order of 10^{-6} cause a transient decrease in stiffness in nonlinear elastic materials.

Anthropogenic activities on the field-scale such as drilling, wastewater storage, hydraulic fracturing result in considerable deformation of reservoir rocks. Changing the hydromechanical properties by dynamic stressing from fluid injection are likely to present hazards in the form of fault reactivation and reservoir seal damage. Evidence of this type of stressing inducing regional seismicity is rich and numerous (*more details and citations*). Despite the hazards, dynamic stressing of the subsurface may result in enhanced permeability, consequently greater energy recovery. Seismic and anthropogenic sources of dynamic perturbation both change rock stiffness and permeability in similar ways, which suggests there is a physical mechanism that relates the nonlinear stiffness and poromechanical properties of fractured rock.

Nonlinear response is sensitive to many fracture properties: geometry, flow pathways, asperity compliance, and friction. Currently, literature for investigating the relationship b/w elastodynamic and poromechanical and subsequent recovery is quite limited. We present the results from sophisticated well-controlled laboratory experiments in which we combine the analysis of nonlinear elastodynamic and hydraulic data.

It is expected that the nonlinear behavior of rocks is sensitive to fine features such as fracture aperture (i.e. flow pathways, asperity stiffness). In order to fully understand the ramifications of dynamic stressing in the subsurface, we need elucidate the relationship between the elastodynamic and hydro-mechanical properties of fractured rocks.

4 Experimental Setup

We conducted sophisticated experiments in which samples were loaded under triaxial conditions inside a pressure vessel and fractured in-situ to simultaneous measure flow rate and elastic properties. Westerly granite samples were prepared by cutting them into L-shape blocks (69 x 45 50 x 26 mm, Figure 1) with 3 mm deep notches on the top and bottom to ensure reproducibility of planar fracture propagation. The L-shape is used for maintaining constant nominal contact area during fracture and shear. The samples were saturated in deionized water and then placed between steel forcing blocks that have embedded piezoelectric transducers. The P-polarized lead-zirconate transducers (PZTs) of company APC International Ltd. are 6.5 mm in diameter, with a center frequency of 500 kHz and the spacing between the steel loading platen and the PZTs is 4mm. The shorter forcing block additionally contains internal conduits to provide fluid flow along the fracture plane. Deionized water was pumped through these narrow channels (45 x 1 mm) and covered by sintered porous fits and fed by five 1.6 mm diameter holes. Sintered porous frits (permeability 10^{-14} m^2) are press-fit into cavities within the short forcing block to allow homogenous distribution of fluid. After securing this Single Direct Shear (SDS) configuration, it was sealed inside a latex jacket to separate confining and pore fluids. Fully prepared and jacketed samples were fitted inside a pressure vessel within a biaxial loading apparatus.

The Biax consists of two hydraulic pistons capable of applying vertical and horizontal loads in displacement or load control. Forces are measured using custom-built, beryllium-copper strain-gauge load cells mounted on each loading piston. The load cells have an amplified output of $\pm 5 \text{ V}$ with an accuracy of $\pm 5 \text{ N}$ and are calibrated with a Morehouse proving-ring. Displacements are measured with direct-current displacement transducers (DCDT), with an accuracy of $\pm 0.1 \mu\text{m}$. The confining fluid, a food-grade heat transfer oil (XCELTHERM 600, Radco Industries), in the sealed pressure vessel is pressurized to create a true-triaxial stress conditions. A linear variable differential transformer was attached to the outside of the sample, inside the pressure vessel, to accurately ($\pm 0.1 \mu\text{m}$) measure the fracture displacement. Pressure intensifiers fitted with LVDTs and pressure transducers were used to control the confining pressure and the internal upstream and downstream pressures.

Each axis of loading is independently servo-controlled and all stresses, strains, fluid pressures and fluid volumes were recorded with $\pm 10 \text{ V}$, 16-channel 24-bit analog-to-digital converter at 10 kHz and averaged to sampling rates of 100 Hz or 1 kHz. Fracture permeability was measured using upstream and downstream pore-pressure intensifiers. Active ultrasonic data were recorded using a VantageTM Research Ultrasound (Verasonics) system. We use broadband (0.02-2 MHz) PZTs (APC International Ltd. 6.35 diameter

compressional crystals), which were successively pulsed every 1 ms on the transmitting side and the recording rate at the receiver side was 25 MHz. The input signal is a half sine with a frequency of 500 kHz. Also, a pulse from the Verasonics system accompanied the PZT excitation and is recorded by the 24-bit analog-to-digital data acquisition system. This allows us to sync the “ultrasonic” to “poro-mechanical” data and then analyzed to measure changes in the permeability and elasticity of the fractured rock samples, explained more fully in the signal analysis procedure.

Before commencing each experiment, the samples were installed in the pressure vessel and then the vessel was sealed and then filled with confining fluid. A horizontal load of 20 MPa was applied and then the confining fluid pressure was slowly increased to 15 MPa; it is important to monitor the integrity sample jacket seal during this step. Next, we applied a pore pressure differential: inlet ($P_{pA} = 4$ MPa) and outlet ($P_{pB} = 2$ MPa). At this point there was no flow because Westerly granite matrix permeability is very low ($< 10^{-20} \text{ m}^2$) and the confining fluid pressure is greater than the pore pressure (there was no flow around the sample). After establishing all loads and pore pressure, the ultrasonic data acquisition Once all fluid pressures and solid stresses were applied, the ultrasonic data acquisition system (Verasonics®) was started. The sample was then fractured *in situ* by increasing the shear stress at constant normal stress while making continuous measurements of fluid flow and ultrasonic properties. After locking the vertical piston (no displacement allowed), we executed the dynamic stressing protocol illustrated in Figure 2a.

After executing the normal stress and pore pressure oscillation protocol, the fractured sample was sheared twice in 4 mm increments (for a total of 8 mm). During the shearing phases of the experiment acoustic emissions (AEs) were monitored (passive source recording). Subsequent to shearing the dynamic stressing protocol was repeated. We incorporate shearing in this investigation to determine its influence on the non-linearity measurements of the fracture. The fracture aperture is changed through shear, in effect, modeling the complexity of fractured subsurface rock.

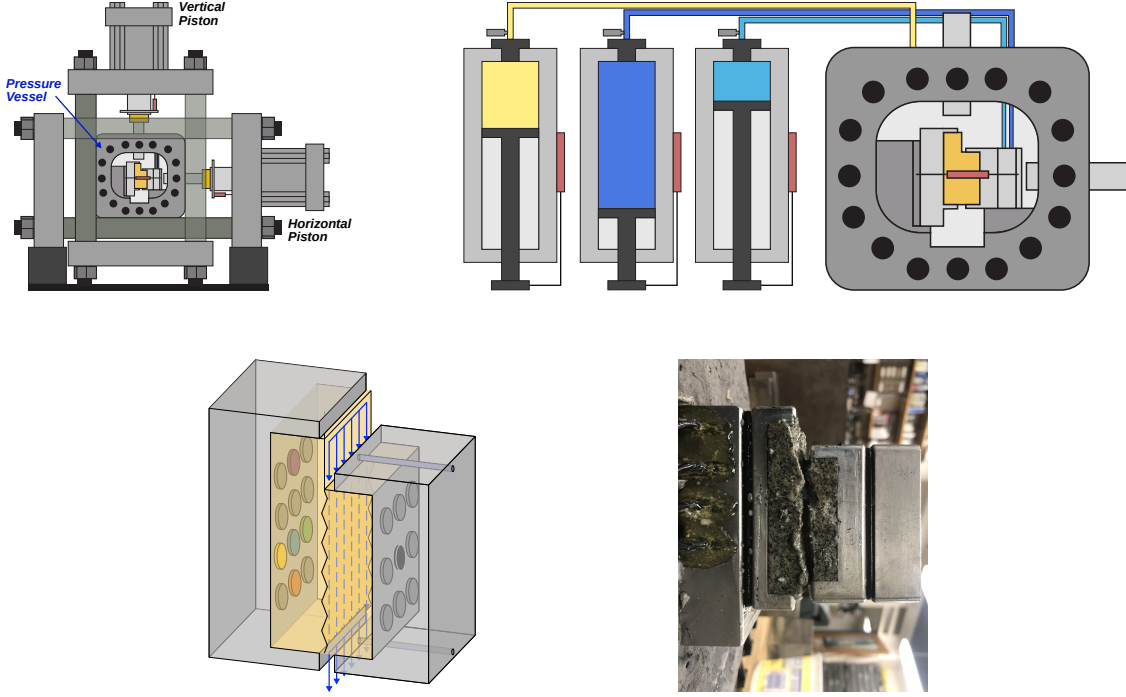


Figure 1: (a) The experiments were conducted in the Penn State Rock and Sediment Mechanics laboratory using the Biaxial Deformation Apparatus (Biax). The Biax has servo-controlled vertical and horizontal pistons and a 10 kHz 24-bit analog to digital data recorder. (b) A pressure vessel was inserted in the Biax and connected to the pressure intensifiers, which control the confining (P_C), and sample (P_{PA} and P_{PB}) fluid pressures. (c) The Westerly granite sample is machine cut into a L-shape and placed between the two loading platens. These loading platens are embedded with piezoelectric transducers (p-polarized) and contain fluid ports for the inlet and outlet flow. The shorter forcing block additionally contains internal conduits to provide fluid flow along the fracture plane. Deionized water was pumped through these narrow channels (45×1 mm) and covered by sintered porous fits and fed by five 1.6 mm diameter holes. Sintered porous frits (permeability $\sim 10^{-14} \text{ m}^2$) are press-fit into cavities within the short forcing block to allow homogeneous distribution of fluid. After securing this Single Direct Shear (SDS) configuration, it was sealed inside a latex jacket to separate confining and pore fluids. (d) A photo of the sample after experimentation highlights the degree of roughness of the in-situ fracture.

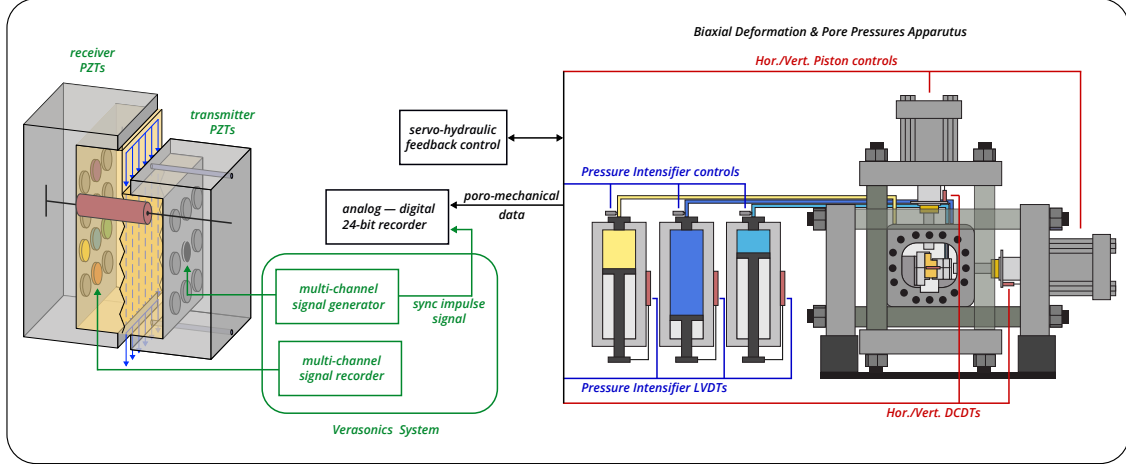


Figure 2: Schematic of the single direct shear configuration with the block diagram showing the main features of the data acquisition system for both the poro-mechanical and ultrasonic data. The Biax consists of two hydraulic pistons capable of applying vertical and horizontal loads in displacement or load control. Forces are measured using custom-built, beryllium-copper strain-gauge load cells mounted on each loading piston. The load cells have an amplified output of 5 V with an accuracy of 5 N and are calibrated with a Morehouse proving-ring. Displacements are measured with direct-current displacement transducers (DCDT), with an accuracy of $\pm 0.1\mu\text{m}$. Each axis of loading is independently servo-controlled and all stresses, strains, fluid pressures and fluid volumes were recorded with 10 V, 16-channel 24-bit analog-to-digital converter at 10 kHz and averaged to sampling rates of 100 Hz or 1 kHz. Fracture permeability was measured using upstream and downstream pore-pressure intensifiers. Active ultrasonic data were recorded using a Vantage TM Research Ultrasound (Verasonics) system. We use broadband (0.02-2 MHz) PZTs (APC International Ltd. 6.35 mm diameter compressional crystals), which were successively pulsed every 1 ms on the transmitting side and the recording rate at the receiver side was 25 MHz. The input signal is a half sine with a frequency of 500 kHz. Also, a pulse from the Verasonics system accompanied the PZT excitation and is recorded by the 24-bit analog-to-digital data acquisition system. This allows us to sync the ultrasonic to poro-mechanical data and then analyzed to measure changes in the permeability and elasticity of the fractured rock samples, explained more fully in the signal analysis procedure.

4.1 Dynamic Effective Stress Perturbations

The fractured samples were dynamically perturbed via pore pressure (P_P) and normal stress (σ_n) oscillations. Following the procedure described by Candela et al., 2015, pore pressure oscillations were achieved by oscillating P_{PA} while holding P_{PB} constant. Conversely, normal stress oscillations were applied by oscillating the horizontal piston of the load frame at prescribed amplitude and frequency. As depicted in Figure 2a, multiple sets of P_P and σ_n oscillations of varying amplitude (up to about \pm MPa) and frequency (0.1, 1, 10 and 40 Hz) were applied to investigate the repeatability as well as amplitude and frequency dependencies of the measured response. Similar parameters were used for P_P and σ_n oscillation sets in order to apply similar effective stress perturbations and allow making comparisons between P_P and σ_n stimulations.

4.2 Permeability Measurements

We measured flow rates independently at the inlet (Q_A) and outlet (Q_B) using the outputs of LVDTs on the pressure intensifiers. After verifying the steady state flow condition ($Q_A - Q_B \leq 5\%$), Darcy's law was used to calculate permeability k :

$$k = \frac{\mu L}{S} \frac{Q}{\Delta P_P} \quad (1)$$

where $Q = \frac{1}{2}(Q_A + Q_B)$ is the average flow rate ($\frac{m^3}{s}$), μ is the fluid viscosity ($10^{-3} Pa \cdot s$) at $20^\circ C$, L is the flow path given by the length of the sample (50 mm) and S is the cross section perpendicular to the flow path (45 x 26 mm^2).

Specifically, k is the bulk permeability, that is, the permeability of the surrounding rock matrix (on order of $10^{-21} m^2$) and of the fracture [Zhang et al., 2017; Ishibashi et al., 2018]. Alternative calculations of permeability are valid [Zhang et al., 2017; Ishibashi et al., 2018], however we are interested in relative changes in permeability in response to dynamic stressing, so the absolute value of the permeability is not necessary to quantify.

4.3 Ultrasonic Measurements: Active Source

Ultrasonic waves transmitted through the fracture were recorded continuously in each experiment. Half-cycle sinusoidal pulses with an amplitude of 40 V and center frequency of 500 kHz were emitted consecutively from each transmitting transducer (9 piezoelectric discs arranged in a 3 x 3 matrix embedded within the right-hand loading block in Figure 1b) with a pulse repetition frequency (PRF) of 100 Hz or 1000 Hz during the low and high frequency (≥ 10 Hz) stress oscillations, respectively. The waveforms were amplified (~ 40 dB) and recorded for all the receiving transducers (12 piezoelectric discs arranged in a 4 x 3 matrix embedded within the left-hand loading block in Figure 1b). We activated up to the full array of 9 transmitter and 12 receivers.

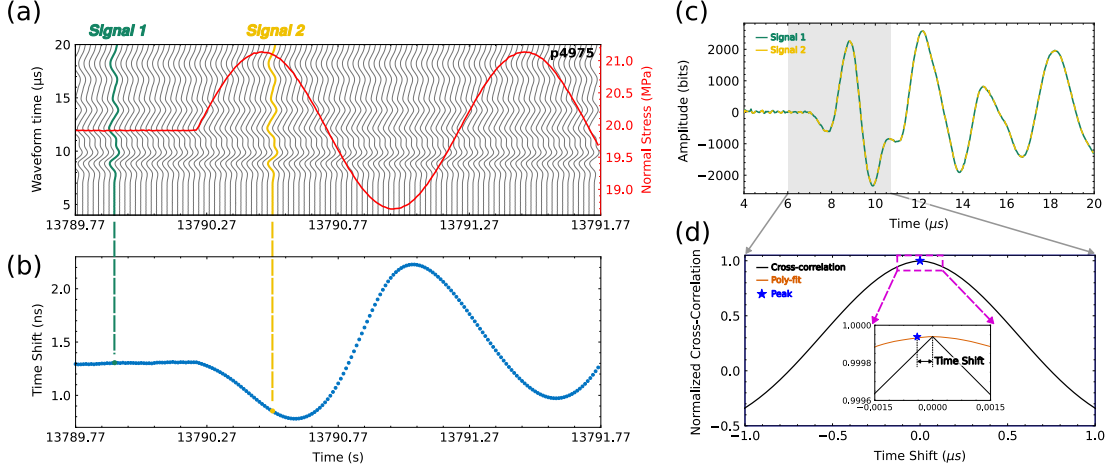


Figure 3: (a) Excerpt from run4 of experiment p4966 shows part of a 1 Hz, 1 MPa normal stress oscillation (red) and the concurrent raw ultrasonic waveforms (grey). The number of waveforms in the waterfall plot has been decimated version for clarity. (b) Time shift was calculated by cross-correlating the waveforms to a reference waveform. (c) An example of a reference, unperturbed, waveform (green) and perturbed waveform (dashed yellow) highlights the similarity. (d) The maximum linear correlation between the reference and perturbed waveforms from cross-correlation is used to determine the time shift. The inset shows improvement of time shift calculations with a 2nd order polynomial fitting procedure.

5 Experimental Procedure

Each experiment commenced with extensive sample preparation: in which the Westerly granite was cut and notched, sealed in a latex jacket, and then placed inside the pressure vessel (see Section 4 for details). After sealing the pressure vessel and loading the sample, inlet and outlet flow were pressurized to 4 MPa and 2 MPa, respectively. At this stage there was no flow because Westerly granite matrix permeability is very low ($< 10^{-20} \text{ m}^2$) and the confining fluid pressure (around the jacketed sample) is much larger than the pore pressure, preventing flow of water around the sample. A shear load was then applied with the vertical piston in displacement mode at a constant $10 \mu\text{m/s}$, fracturing in-situ after reaching a critical stress of $\approx 60 \text{ MPa}$, and then locked the vertical piston. During fracture fluid flow and acoustic emissions were measured, but these results are not included in this paper. Next, the dynamic stressing protocol was implemented in which the normal stress and pore pressure were modulated. Normal stress oscillations were applied by oscillating the horizontal piston of the load frame at prescribed amplitudes (0.2 to 3 MPa) and frequencies (0.1, 1, 10, 40 Hz). Pore pressure oscillations were achieved by oscillating P_{PA} while holding P_{PB} constant at amplitudes of 0.2 to 3 MPa and frequencies of 0.1, 1, 10 Hz. Multiple sets of normal stress and pore pressure oscillations of varying amplitudes and frequencies were applied to investigate: (1) repeatability and direct comparison between the two modulated stresses and (2) amplitude and frequency dependencies of the measured response. Post-fracture dynamic stressing is plotted in Figure 4d (highlighted in yellow) and shows the normal stress (red) and pore pressure (blue) oscillations; note that line thickness correlates with oscillation frequency. To investigate the effect of fracture aperture on elastic nonlinearity and permeability, the sample was sheared in two 4 mm, (held at $\sigma_{NS} = 20 \text{ MPa}$) stages. After each shearing stage the oscillation protocol was applied to the sample. Initially, the in-situ fracture was quite rough, but the effect of shear reduces and changes this roughness; the old contacts were broken and new contacts formed, changing the extent to which the two halves of the fracture were mated. This allows for investigation of how fracture aperture is related to the elasto-dynamic and hydromechanical properties.

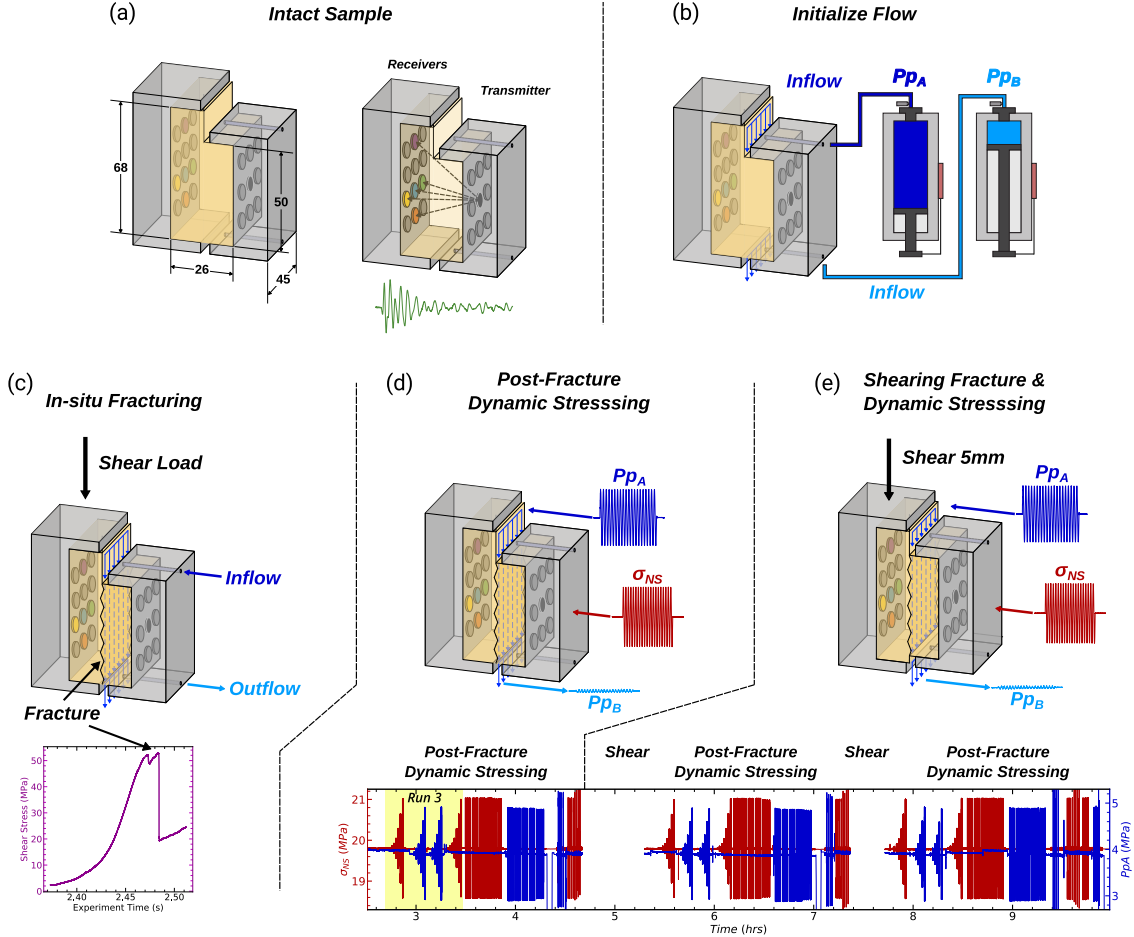


Figure 4: (a) Intact Westerly granite sample cartoon, showing dimensions and approximate transmitter - receiver ray paths. (b) Next, we applied a pore pressure differential: inlet ($P_{pA} = 4$ MPa) and outlet ($P_{pB} = 2$ MPa). (c) The shear stress was loaded at a constant rate of $10 \mu\text{m}/\text{s}$ until reaching the critical shear stress at ≈ 60 MPa. (d) Cartoon showing the oscillation protocol applied to the freshly fractured sample. Multiple sets of P_P and σ_{NS} oscillations of varying amplitude (up to about ± 1 MPa) and frequency (0.1, 1, 10 and 40 Hz) were applied. (e) The sample was sheared in two additional increments of 4mm, each followed by the dynamic stressing protocol.

6 Results

As previously specified, the ultrasonic waveforms are combined with strain measurements to calculate the nonlinear elastodynamic response and flow rates are used to determine fracture permeability. These measurements allow us to ascertain how the in-situ fracture responds to dynamic stressing. In other words, the imposed oscillations that range in amplitude and frequency probe the elastodynamic and hydraulic properties of the fractured samples. Subsequent results derive from two separate experiments.

6.1 Nonlinear elastodynamic and hydraulic responses

Through our active source ultrasonic monitoring we characterize the elastodynamic properties of the fractured Westerly granite by quantifying its response to dynamic stressing. Figure 5 demonstrates typical elastodynamic and hydraulic changes in response to a 1 Hz, 1 MPa normal stress oscillation in experiment number p4966. We characterize the elastodynamic response with three parameters to describe the nonlinearity, $\Delta c/c_0$, dc/c_0 , and \dot{c} . We observe that before oscillation the wave velocity c_0 is steady-state and immediately following an oscillation the velocity instantaneously decreases. That is to say, the fractured rock stiffness of decreases in response to dynamic stressing, quantified by the parameter $\Delta c/c_0$. Another nonlinearity parameter that we identify is modulation in the wave velocity during oscillations at frequencies that are harmonics of the driving frequency. dc represents the average amplitude of these modulations of the wave velocity during dynamic perturbations. Finally, after the stressing the fractured rock exhibits long-term slow dynamics "recovery" to the initial c_0 value, in which the wave velocity evolves to a new, non-equilibrium, steady-state. The rate of wave velocity evolution from post-oscillation to initial c_0 is fitted with a logarithmic function of the form $\dot{c} = p_1 \log t + p_2$, where p_1 is the slope (recovery rate) and p_2 is the intercept.

For the purpose of illustration, linearly elastic media (of which rocks are not) wave propagation is stress-invariant. Undamaged, unperturbed, rocks do exhibit a modicum of nonlinearity due to microcracks in their matrices and soft grain boundaries (Rivière et al., 2015). When fractured or damaged, rock nonlinear elasticity is furthermore affected by contact acoustic nonlinearity (CAN) at these rough interfaces. The characteristic responses to dynamic stressing (transient softening, velocity modulation, and slow recovery) as shown in Figure 5, are indicative of nonlinear mesoscopic elasticity (Guyer and Johnson, 2009) and highly informative on rock microstructure, fractures, and contact mechanics.

The stress-induced changes in permeability are captured by two parameters: (1) The transient change in permeability $\Delta k/k_0$ defined as the %-change due to the imposed normal stress or pore pressure oscillations, normalized by the pre-oscillation permeability k_0 as illustrated in Figure 5c (Candela et al., 2014) and (2) the recovery rate of permeability after the transient increase \dot{k} . The recovery rate of fracture permeability is quantified by fitting a logarithmic function to the post-oscillation permeability data over a window of 60s. The data is fit to the equation $\dot{k} = q_1 \log t + q_2$, where q_1 is the slope (recovery rate) and q_2 is the intercept. Permeability during dynamic stressing cannot be quantified because there is not steady-state flow and the diffusion time across the fracture is slower than the larger oscillation frequencies (10 Hz).

To more fully illustrate how the elastodynamic and hydraulic properties of fractured rock change in response to dynamic perturbation we show an excerpt from the post-fracture stage of experiment p4975 in Figure 7. This shows the normal displacement, inlet and outlet flow rates, and wave velocity before, during, and after a 0.1 Hz, 1 MPa normal stress oscillation. Note that inlet and outlet flow rates Q_A and Q_B are not at steady-state during the oscillation, indicated by the phase and amplitude difference. There are three inset plots of Figure 7 that plot the relationship between wave velocity and outlet flow rate Q_A during a full wavelength at the beginning, middle, and end of the normal stress oscillation. These hysteresis plots also show how the wave velocity vary as a function of stress. Throughout this long oscillation the velocity-flow hysteresis loop generally evolves to a lower velocity and lower flow rate and the loop becomes more closed. We also observe this general decrease in wave velocity as a function of applied stress throughout the history of the oscillation. These observations demonstrate the magnitude of changes we are characterizing and also

reinforce that the fracture is continuously evolving during the dynamic perturbations; contacts undergo compression and tension resulting in changing flow paths across the fracture.

In subsequent sections we discuss how nonlinear elastodynamic and hydraulic parameters $\Delta c/c_0$, dc/c_0 , \dot{c} , $\Delta k/k_0$, and \dot{k} vary with normal stress and pore pressure oscillation amplitudes and frequencies. We also discuss how these results are affected by shearing for both experiments p4966 and p4975.

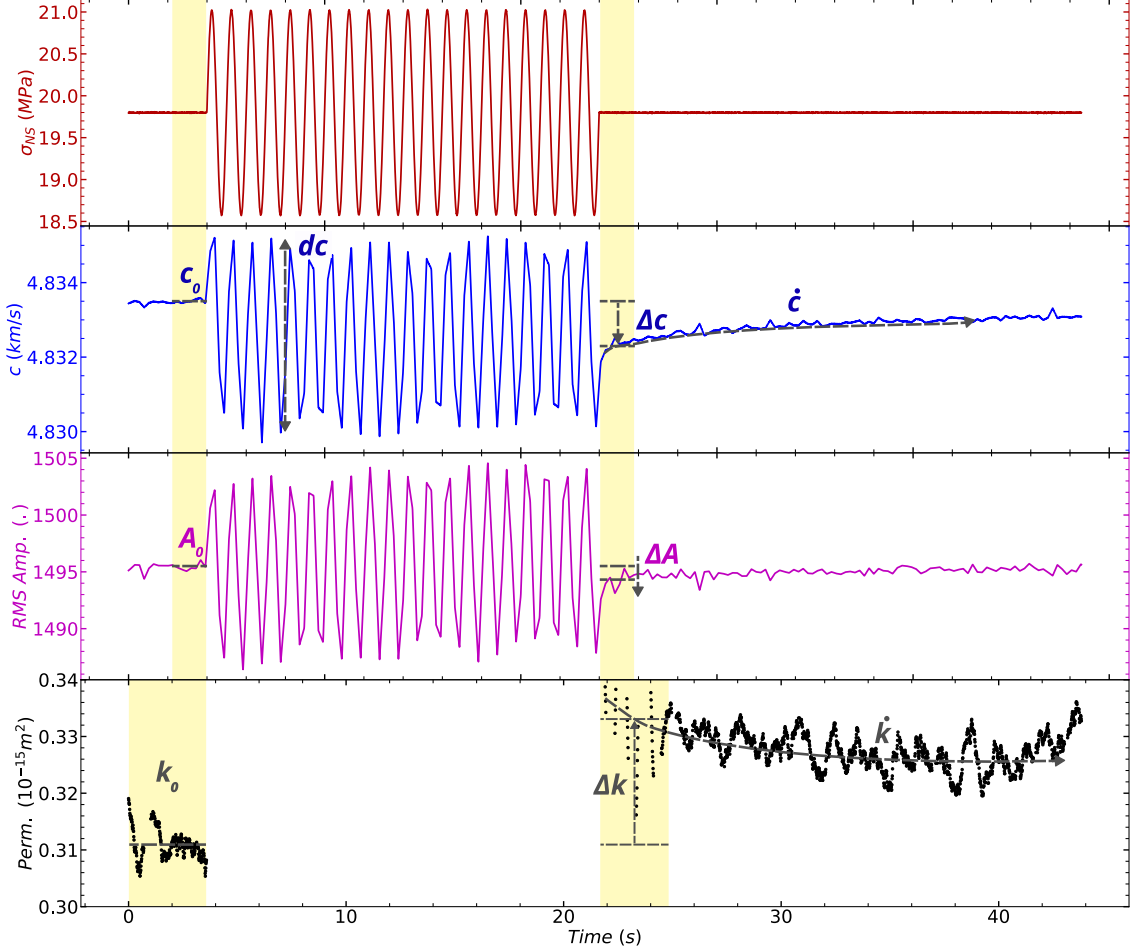


Figure 5: The velocity and permeability changes are calculated using the measured values before and after each oscillation averaged over the time windows (gray boxes) shown in (c). Data points in the permeability measurements are omitted on the condition that inlet/outlet flow rates differ $> 5\%$. That is to say, plotted permeability points represent when there is steady-state flow, necessary for Darcy's law. Dashed lines indicate the recovery of p-wave velocity (\dot{c}) and permeability (\dot{k}), respectively, from post-oscillation response to new steady-state value. Furthermore, we parameterize the p-wave velocity change dc during the normal stress or pore pressure oscillations, indicated by dashed blue line.

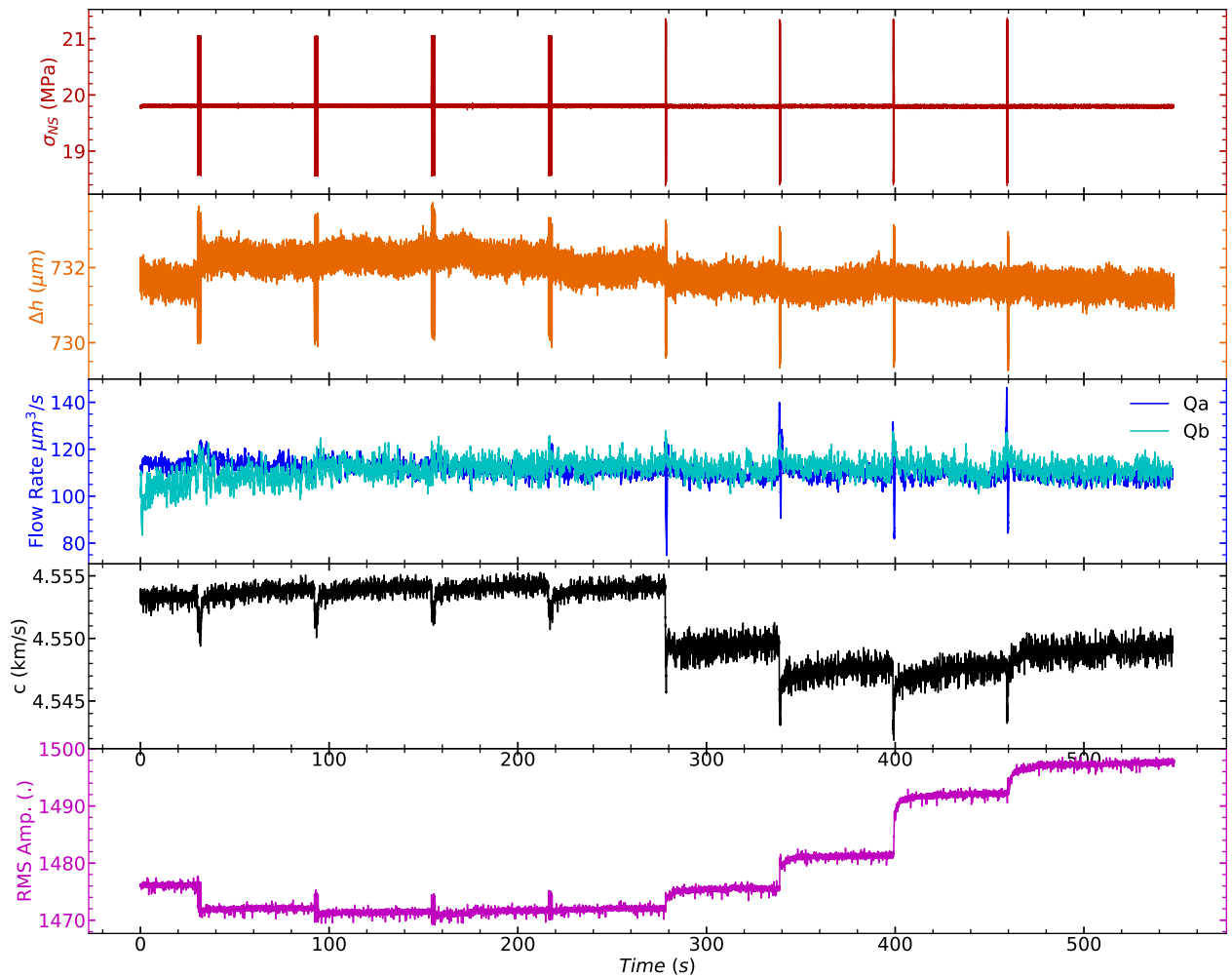


Figure 6: Run 3 of experiment p4975. Trying to figure out how to incorporate this into the main body, maybe move to supplemental.

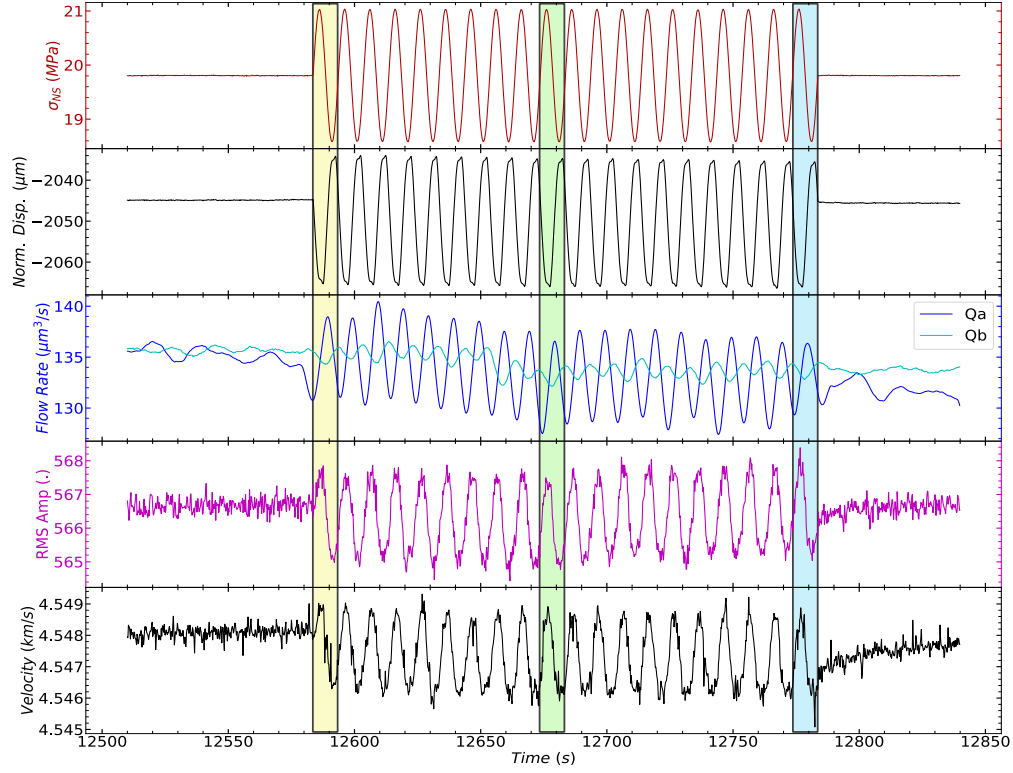


Figure 7: (a) Direct response of normal displacement, flow rate (inlet and outlet), and ultrasonic velocity for the direct path pair during a 0.1Hz 1MPa Normal Stress oscillation. Note the phase delay between the inlet and outlet flow rates. (b) shows how velocity varies as a function of outlet flow rate, Q_b , during the last cycle of the normal stress oscillation. The velocity increases with decreasing flow rate during compression and then the opposite trend with tension. The point to make here is that the fracture is continuously changing – the change in aperture results in change in velocity and flow paths. (c) Ultrasonic velocity as a function of the last full cycle of the normal stress oscillation.

Delineate (b) & (c) to distinguish compression and tension of oscillation.

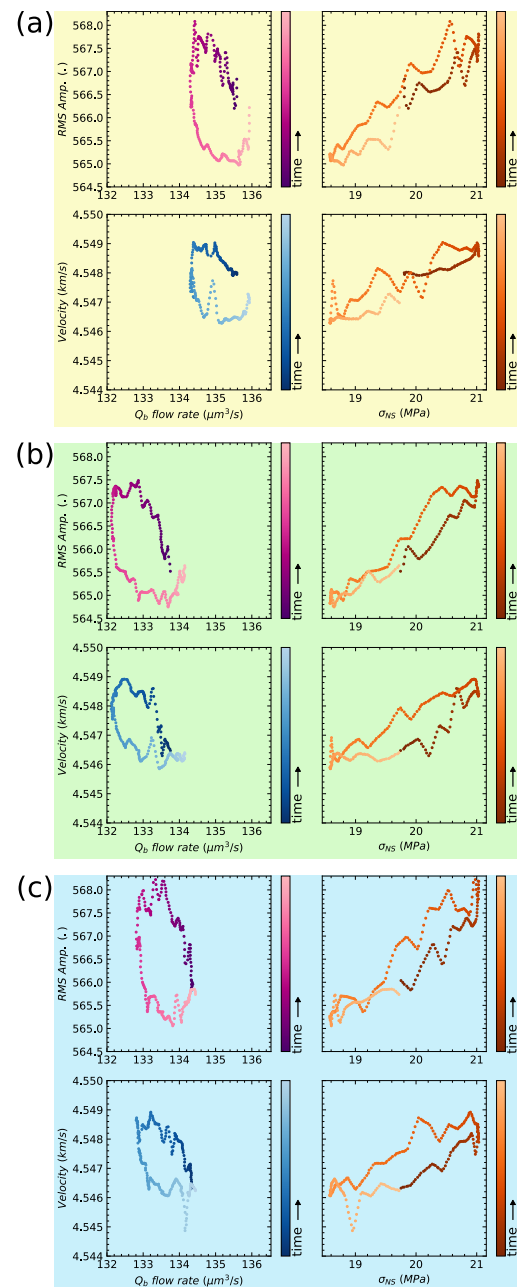


Figure 8

6.2 Nonlinear Elastodynamic Response: Relative Change in Velocity and Permeability

- nonlinearity modulated by oscillation amplitudes
 - nonlinearity and permeability enhancement generally increase with frequency of dynamic stressing.
 - relative changes in wave velocity and permeability are correlated: larger drops in velocity — \downarrow larger increases in permeability
 - changes in permeability are greater at higher oscillation amplitudes
- Perm enhancement pronounced for Pp oscillations than for NS.

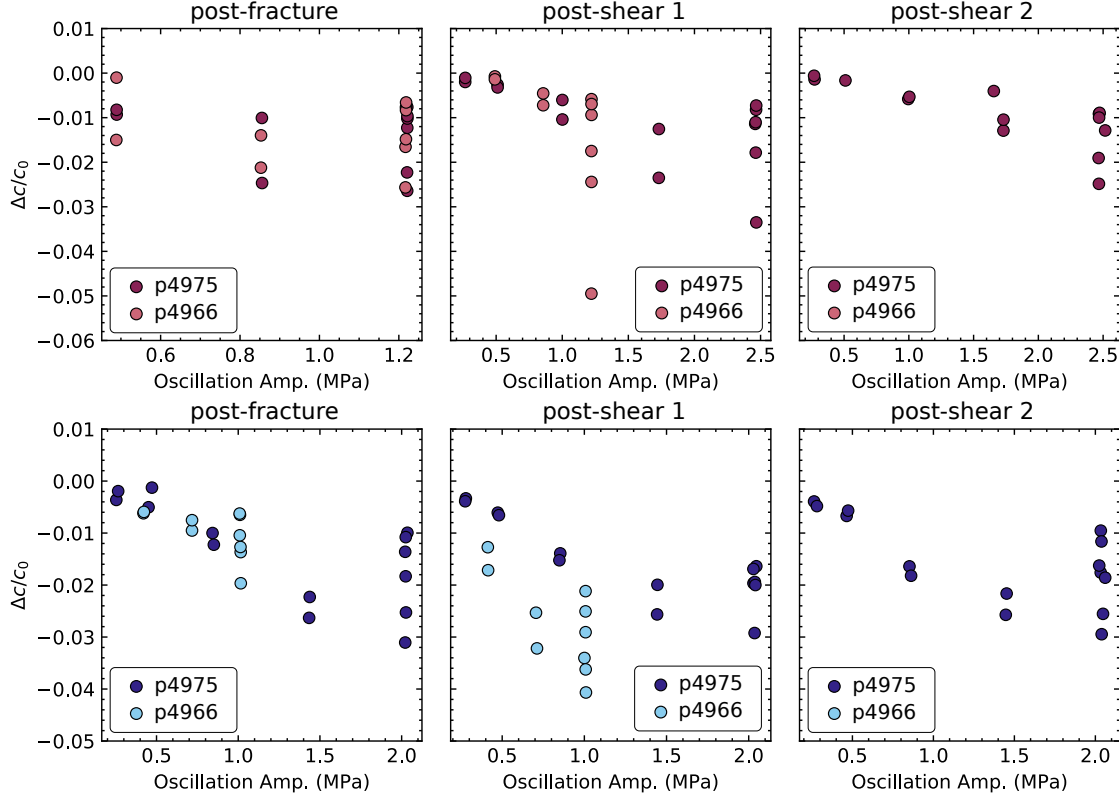


Figure 9: Nonlinearity as a function of σ_{NS} oscillation amplitude. Transitioning from post-fracture results to post-shear results, we observe decreased nonlinearity and permeability enhancement. This is probably related to clogging mechanisms.

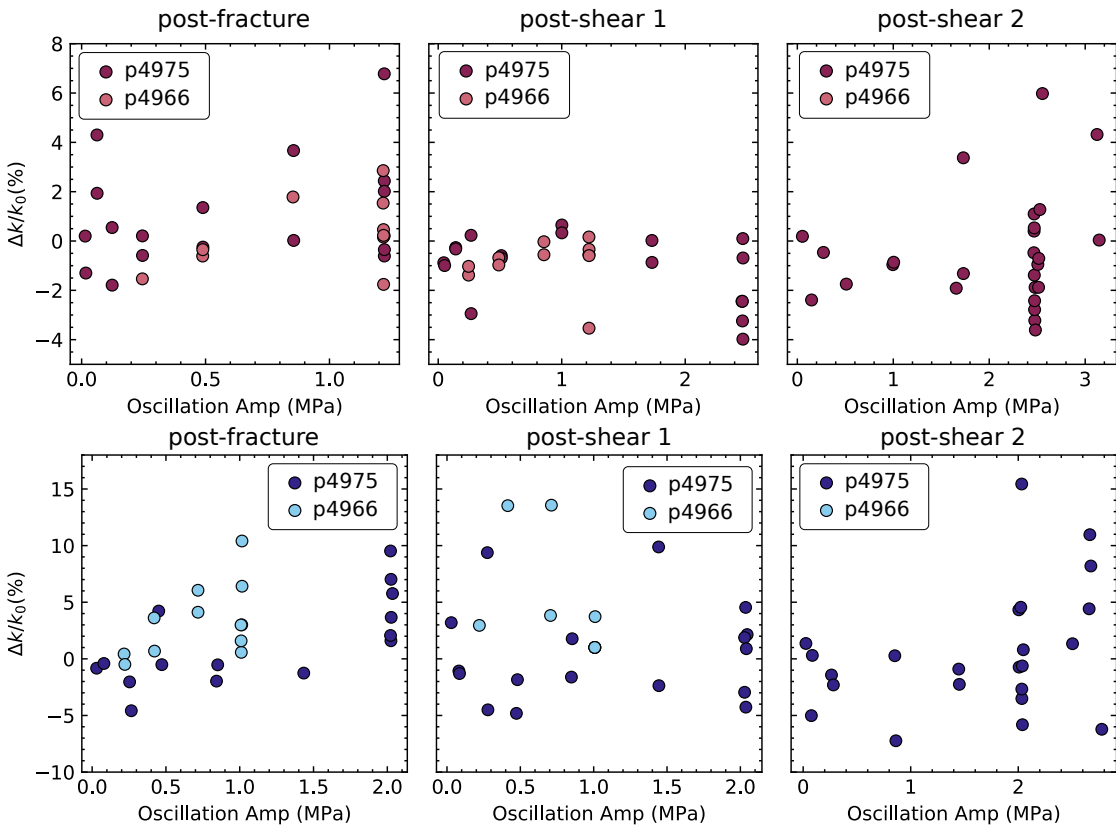


Figure 10: Change in permeability as a function of σ_{NS} oscillation amplitude. Transitioning from post-fracture results to post-shear results, we observe decreased nonlinearity and permeability enhancement. This is probably related to clogging mechanisms.

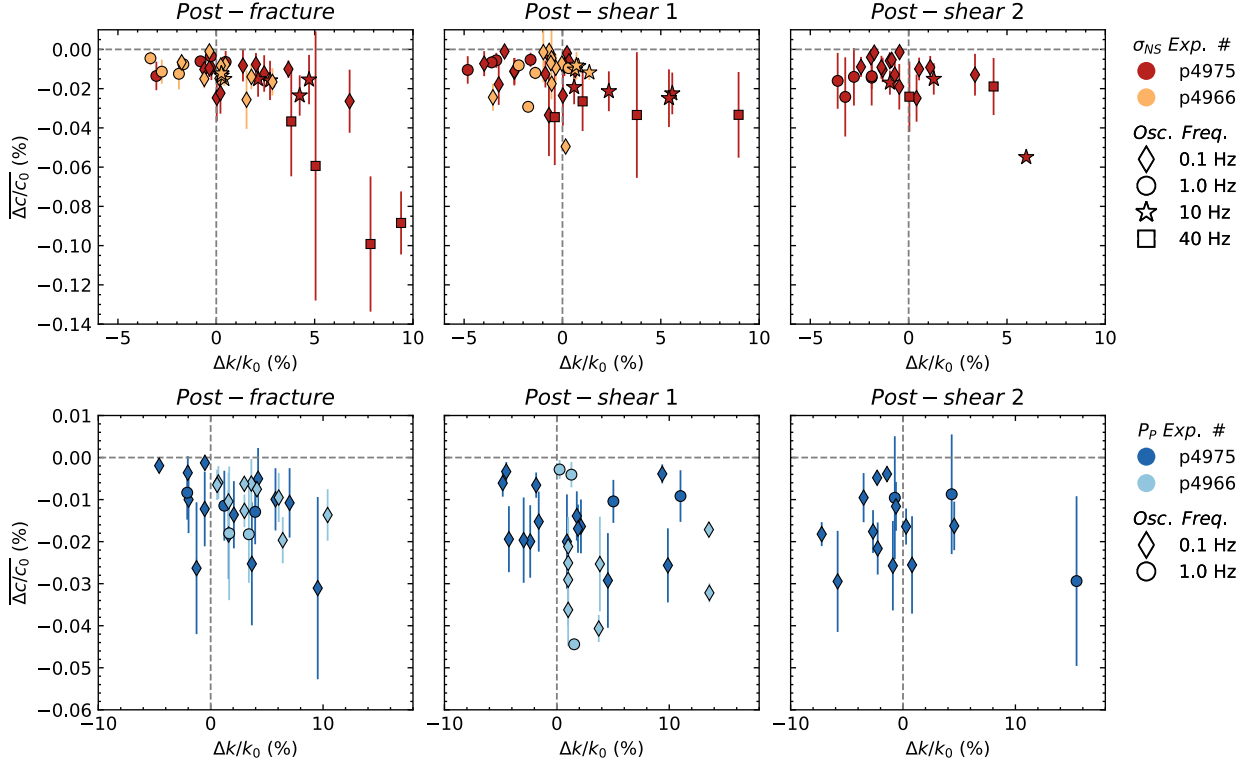


Figure 11: Nonlinearity as a function of permeability change for σ_{NS} and P_p oscillations averaged over all receivers. Permeability is an averaged measurement across the fracture, so these parameters should exhibit some relationship. I don't know what this says about the mechanisms at play. Maybe the contact area has been reduced (lower nonlin) and also maybe wear material was mobilized during P_p oscillation and temporarily increased contact area (higher nonlin). Does this match with reality – does shearing the fracture increase the contact area? My intuition agrees with this, but it is conceivable that with a complex geometry, this could be more complex.

6.3 Velocity Amplitude Modulation during Perturbations

- Although the origins of dc/c_0 and dc/c remain unclear, consider empirical evidence from [Rivière et al., 2015, 2016] that they originate from different micro-scale mechanisms

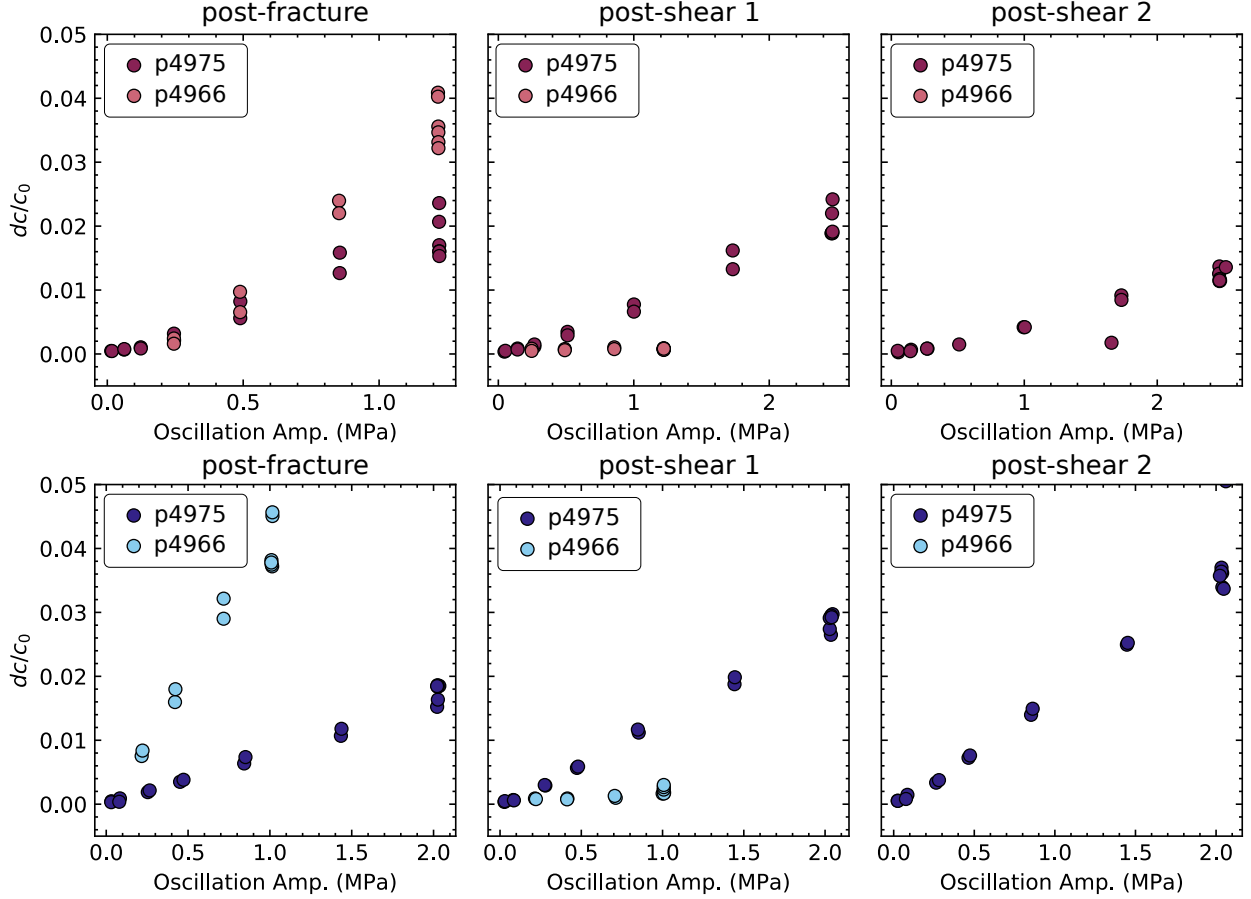


Figure 12: Velocity amplitude modulation averaged over all receivers (dc/c_0) as a function of permeability recovery (k) for NS and PP oscillations. I suspect that we are not waiting long enough to see a trend like J. Elkhouri and others. His recovery values were 0.5, which he says is related to the dimensionality of the fracture. Shearing the fracture increases the complexity and maybe changes the slope – dominated by clogging/moving wear material rather than mated aperture.

6.4 Recovery of Velocity and Permeability

- Although the origins of $\Delta c/c_0$ and dc/c remain unclear, consider empirical evidence from [Rivière et al., 2015, 2016] that they originate from different micro-scale mechanisms

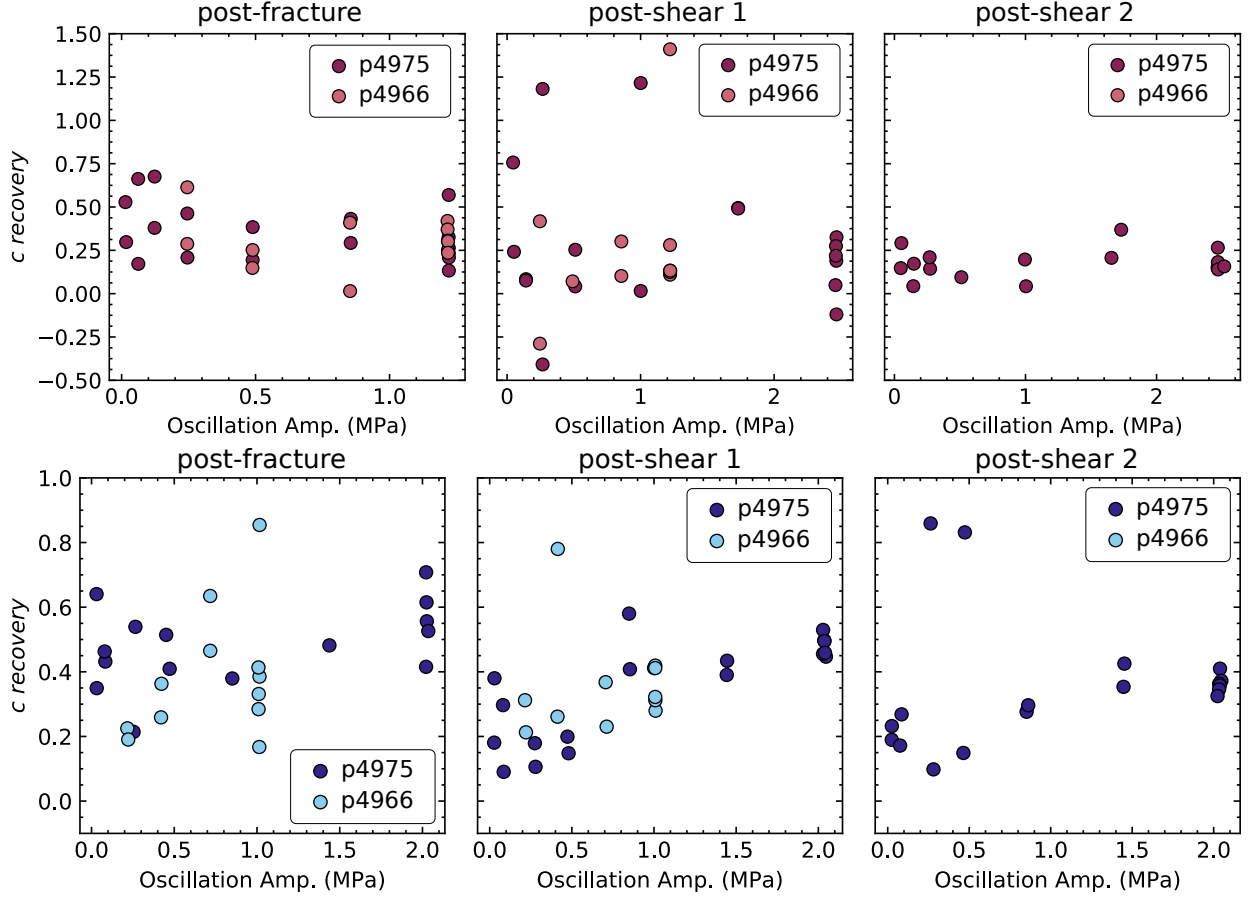


Figure 13: Velocity recovery averaged over all receivers (\bar{c}) as a function of oscillation amplitude for NS and PP oscillations. I suspect that we are not waiting long enough to see a trend like J. Elkhoury and others. His recovery values were 0.5, which he says is related to the dimensionality of the fracture. Shearing the fracture increases the complexity and maybe changes the slope – dominated by clogging/moving wear material rather than mated aperture.

7 Supplemental

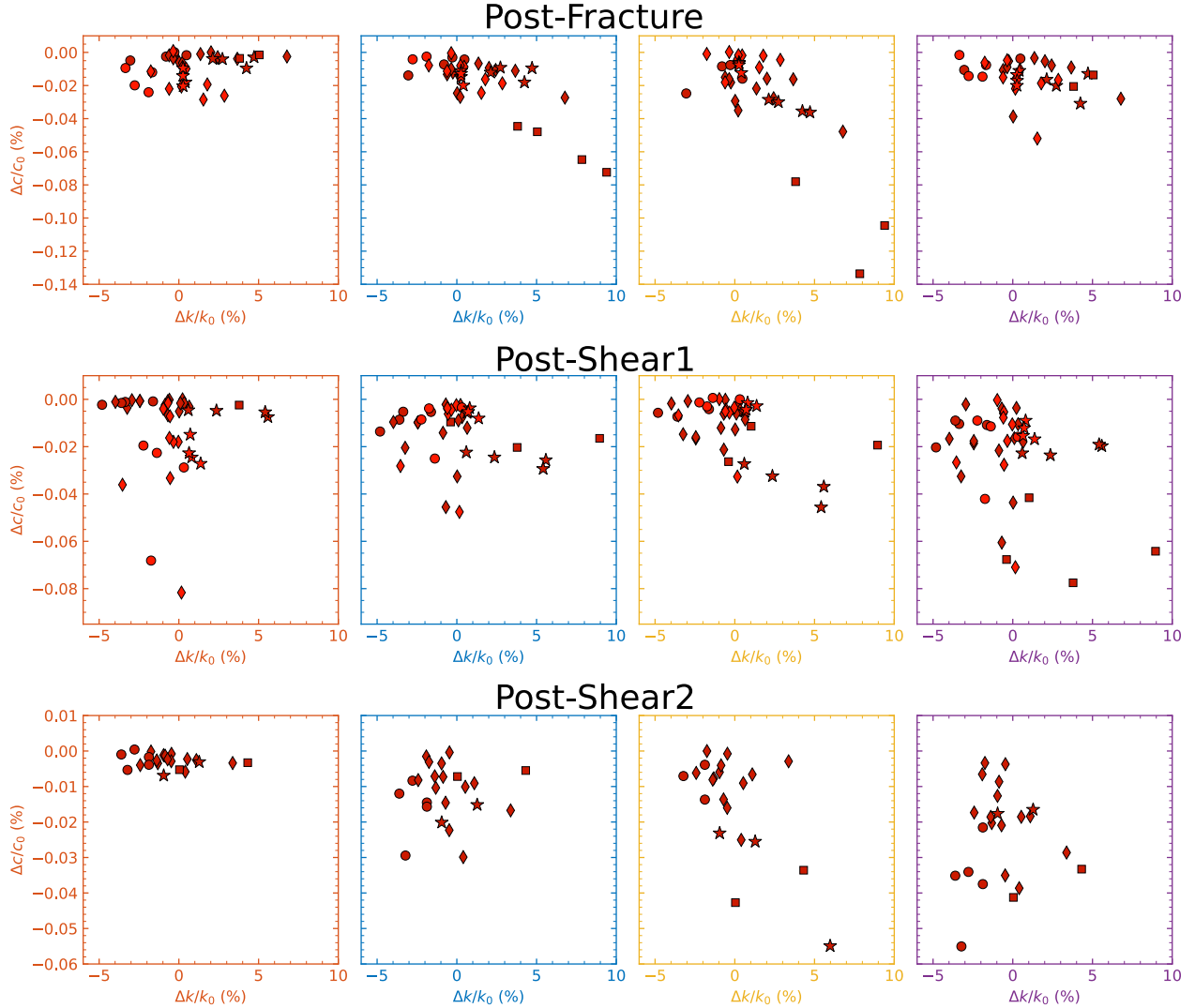


Figure 14: Nonlinearity as a function of permeability change for σ_{NS} oscillations for each receiver. Transitioning from post-fracture results to post-shear results, we observe decreased nonlinearity and permeability enhancement. This is probably related to clogging mechanisms.

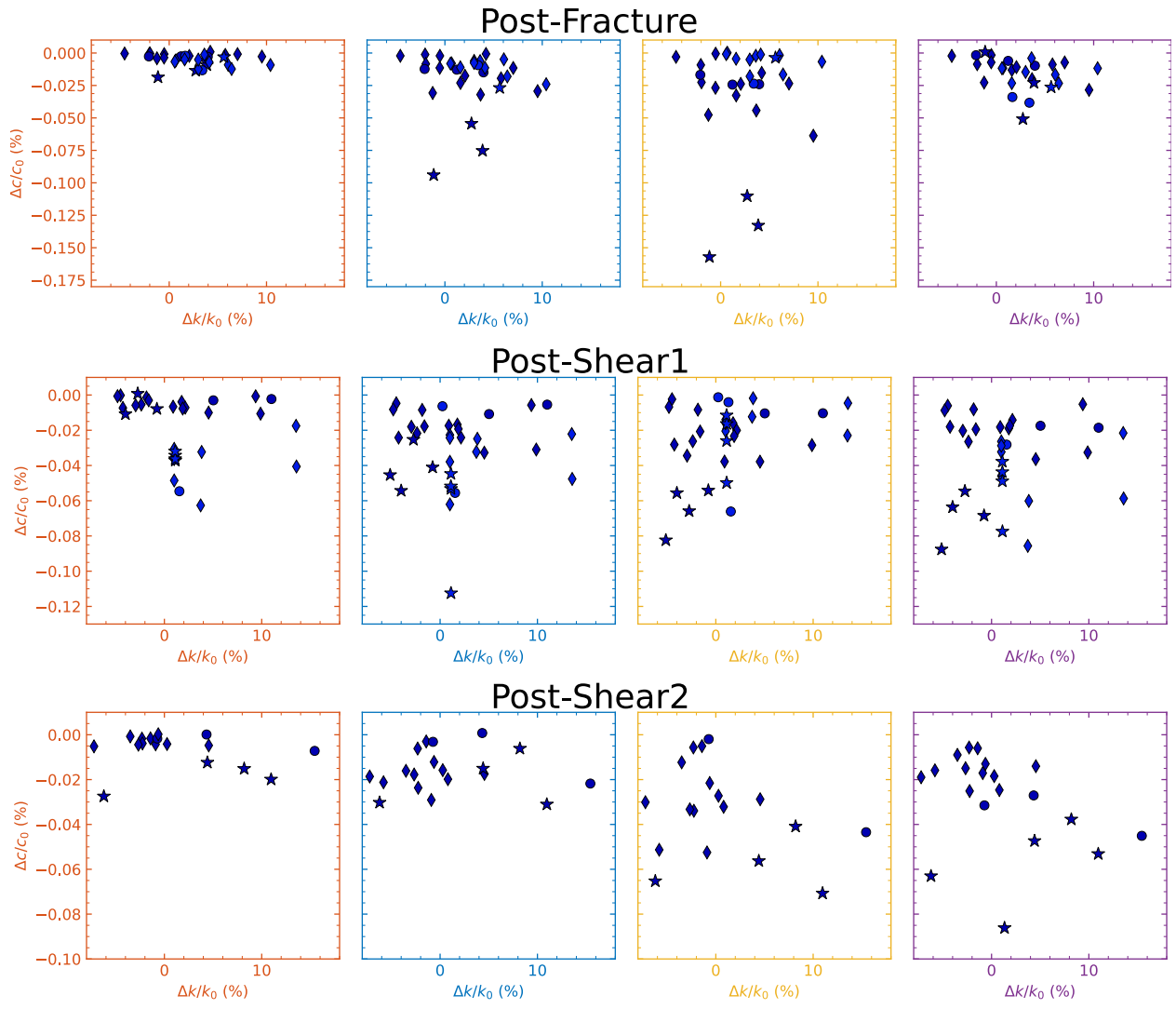


Figure 15: Nonlinearity as a function of permeability change for P_P oscillations for each receiver.

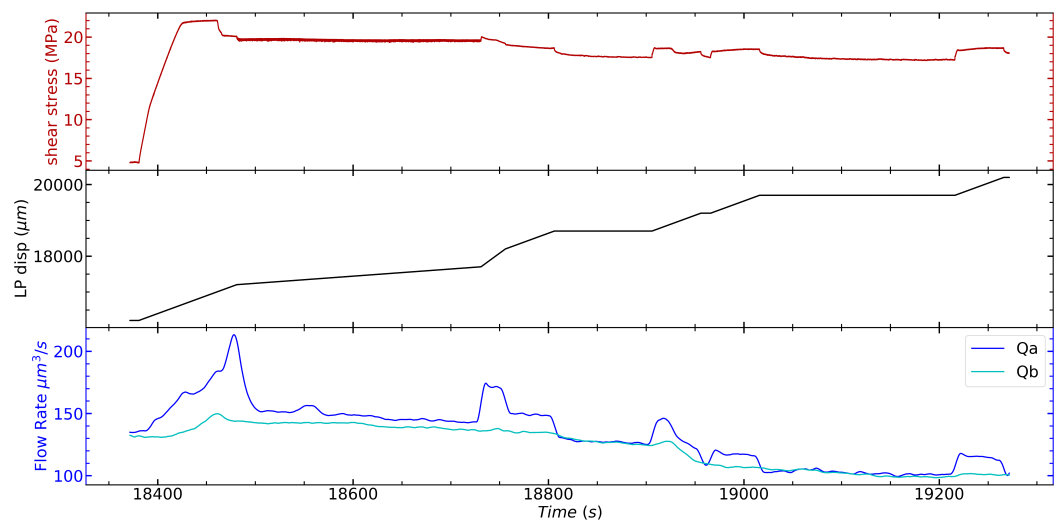


Figure 16: First shearing for p4975.

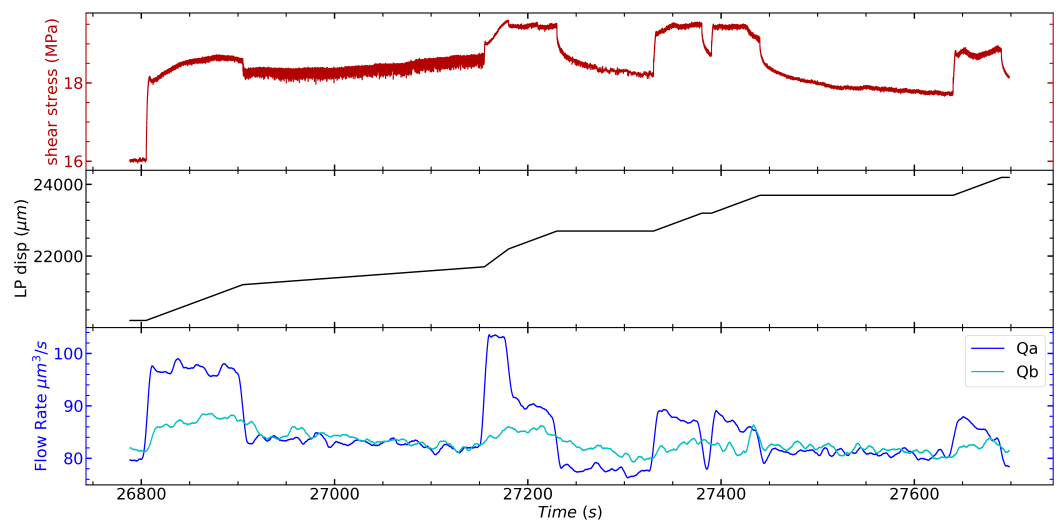


Figure 17: Second shearing for p4975.